The Geometrical Comparisons of RSM and RFM for FORMOSAT-2 Satellite Images

Liang-Chien Chen, Tee-Ann Teo, and Chien-Liang Liu

Abstract

In this paper, we compare the geometrical performance between the rigorous sensor model (RSM) and rational function model (RFM) in the sensor modeling of FORMOSAT-2 satellite images. For the RSM*, we provide a least squares collocation procedure to determine the precise orbits. As for the RFM, we analyze the model errors when a large amount of quasi-control points, which are derived from the satellite ephemeris and attitude data, are employed. The model errors with respect to the length of the image strip are also demonstrated. Experimental results show that the RFM is well behaved, indicating that its positioning errors is similar to that of the RSM.*

Introduction

Sensor orientation modeling is a prerequisite for the georeferencing of satellite images or 3D object reconstruction from satellite stereopairs. Nowadays, most of the high-resolution satellites use linear array pushbroom scanners. Based on the pushbroom scanning geometry, a number of investigations have been reported regarding the geometric accuracy of linear array images (Westin, 1990; Chen and Lee, 1993; Li, 1998; Tao *et al.*, 2000; Toutin, 2003; Grodecki and Dial, 2003). The geometric modeling of the sensor orientation may be divided into two categories, namely, the rigorous sensor model (RSM) and the rational function model (RFM) (Toutin, 2004).

Capable of fully delineating the imaging geometry between the image space and object space, the RSM has been recognized in providing the most precise geometrical processing of satellite images. Based on the collinearity condition, an image point corresponds to a ground point using the employment of the orientation parameters, which are expressed as a function of the sampling time. Due to the dynamic sampling, the RSM contains many mathematical calculations, which can cause problems for researchers who are not familiar with the data preprocessing. Moreover, with the increasing number of Earth resource satellites, researchers need to familiarize themselves with the uniqueness and complexity of each sensor model. Therefore, a generic sensor model of the geometrical processing is needed for simplification. (Dowman and Michalis, 2003).

The RFM is a generalized sensor model that is used as an alternative for the RSM. The model uses a pair of ratios of two polynomials to approximate the collinearity condition equations. The RFM has been successfully applied to several high-resolution satellite images such as Ikonos (Di *et al.*, 2003; Grodecki and Dial, 2003; Fraser and Hanley, 2003) and QuickBird (Robertson, 2003). Due to its simple implementation and standardization (NIMA, 2000), the approach has been widely used in the remote sensing community.

Launched on 20 May 2004, FORMOSAT-2 is operated by the National Space Organization of Taiwan. The satellite operates in a sun-synchronous orbit at an altitude of 891 km and with an inclination of 99.1 degrees. It has a swath width of 24 km and orbits the Earth exactly 14 times per day, which makes daily revisits possible (NSPO, 2005). Its panchromatic images have a resolution of 2 meters, while the multispectral sensor produces 8 meter resolution images covering the blue, green, red, and NIR bands. Its high performance provides an excellent data resource for the remote sensing researchers.

The major objective of this investigation is to compare the geometrical performances between the RSM and RFM when FORMOSAT-2 images are employed. A least squares collocation-based RSM will also be proposed in the paper. In the reconstruction of the RFM, rational polynomial coefficients are generated by using the on-board ephemeris and attitude data. In addition to the comparison of the two models, the modeling error of the RFM is analyzed when long image strips are used.

Rigorous Sensor Models

The proposed method comprises essentially of two parts. The first involves the development of the mathematical model for time-dependent orientations. The second performs the least squares collocation to compensate the local systematic errors.

Orbit Fitting

There are two types of sensor models for pushbroom satellite images, i.e., orbital elements (Westin, 1990) and state vectors (Chen and Chang, 1998). The orbital elements use the Kepler elements as the orbital parameters, while the state vectors calculate the orbital parameters directly by using the position vector. Although both sensor models are robust, the state vector model provides simpler mathematical calculations. For this reason, we select the state vector approach in this investigation. Three steps are included in the orbit modeling: (a) Initialization of the orientation parameters using on-board ephemeris data; (b) Compensation of the systematic errors of the orbital parameters and attitude data via ground control points (GCPs); and (c) Modification of the orbital parameters by using the Least Squares Collocation (Mikhail and Ackermann, 1982) technique.

Center for Space and Remote Sensing Research National Central University, Chung-Li, Taiwan (lcchen@csrsr.ncu.edu.tw).

Photogrammetric Engineering & Remote Sensing
Vol. 72, No. 5, May 2006, pp. 573–579.

0099-1112/06/7205–0573/$3.00/0

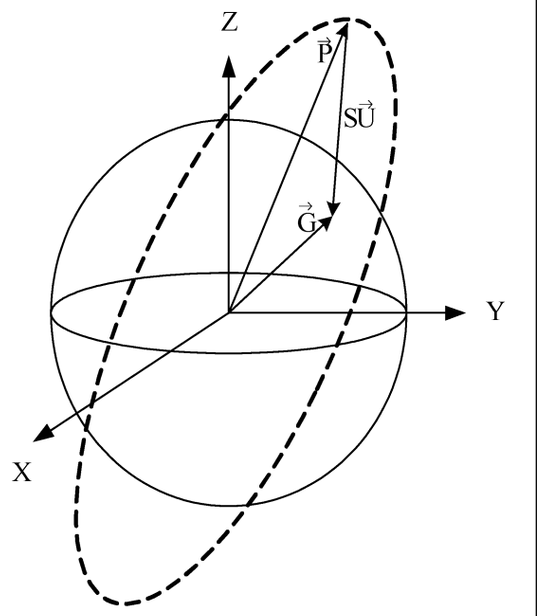

Figure 1. Illustration of State vectors.

The satellite on-board ephemeris data include orbital parameters and attitude data. We use the data to establish the state vectors of satellite positions and the line-of-sight. The state vectors are illustrated in Figure 1, while the collinearity condition equation of state vectors is shown in Equation 1. Once the exterior orientation parameters are formulated, the line-of-sight vector of an image pixel can be calculated. Due to the extremely high correlation between the orbital parameters and attitude data, the two sets of data were iteratively adjusted. As the precision of the sensor position is better than its counterpart, we first use the GCPs to correct the attitude data and subsequently, iteratively adjust the orbital parameters. Equation 2 shows the collinearity condition equation with the attitude correction. The rotation matrix is also formulated to correct the satellite's line-of-sight vectors. The rotation angles are defined in the orbit reference frame, and expressed as second-degree polynomials with respect to the sampling time. In order to compensate the error for orbital parameters, a set of second degree polynomials are applied in this stage (Equation 3).

$$\vec{G} - \vec{P} = S\vec{U} \tag{1}$$

$$\vec{G} - \vec{P} = S \cdot M_Z(\kappa_t) \cdot M_Y(\phi_t) \cdot M_X(\omega_t) \cdot \vec{U} \tag{2}$$

$$\vec{G} - (\vec{P} + \Delta\vec{P}_t) = S\vec{U} \tag{3}$$

where, $\vec{G}$ is the ground point vector, $\vec{P}$ is the satellite position vector, $\vec{U}$ is the satellite line-of-sight vector, S is the scale factor, M_x, M_y, M_z are the rotation matrix, ω_t, φ_t, κ_t are the rotation angles, t is the sampling time, and $\Delta\vec{P}_t$ is the orbital polynomial function.

Least Squares Collocation

Once the trend functions of the orbital parameters are determined, the modification of the orbit is performed by using the Least Squares Collocation. By doing so, we assume that the x, y, and z-axis are independent. Three one-dimensional functions are applied to adjust the orbit. The model of the least squares collocation is shown as:

$$S_k = \sigma_k \cdot \Sigma_k^{-1} \cdot l_k \tag{4}$$

where, k is the x, y, z axis, S_k is the correction value of the interpolating point, σ_k is the row covariance matrix of the interpolating point with respect to GCPs, Σ_k is the covariance matrix for GCPs, and l_k is the residual vectors for GCPs.

The number of GCPs is, in general, insufficient to characterize the covariance function. We, thus, select a Gaussian function with some empirical values for the covariance function, as shown in Equation 5.

$$\Sigma_k = \begin{Bmatrix} (1 - r_n)\mu_k e^{-\left(2.146 \frac{d}{d_{\max}}\right)^2}, & if \quad d \neq 0 \\ \mu_k, & if \quad d = 0 \end{Bmatrix} \tag{5}$$

where, d is distance between an intersection point and a GCP; d_{max} is maximum distance to the intersection point; μ_k is variance of the GCP residual; and r_n is filtering ratio, in the experiment we use 0.2.

This empirical value, 2.146, is selected so that the covariance limit is $1\%*(1 - r_n)\mu_k$, when $d = d_{max}$.

Rational Function Model

The RFM is a generalized sensor model that is considered as an approximate solution for the RSM. The model uses a pair of ratios from two polynomials, as shown in Equation 6, to link the geometry between an image point and the corresponding object point. For high-resolution satellite images that have a small field of view and a high orbit precision, the RFM provides a good approximation in the geometrical processing:

$$\begin{aligned} x &= \frac{p_a(X,Y,Z)}{p_b(X,Y,Z)} = \frac{\sum_{i=0}^{m1}\sum_{j=0}^{m2}\sum_{k=0}^{m3} a_{ijk} X^i Y^j Z^K}{\sum_{i=0}^{n1}\sum_{j=0}^{n2}\sum_{k=0}^{n3} b_{ijk} X^i Y^j Z^K} \\ y &= \frac{p_c(X,Y,Z)}{p_d(X,Y,Z)} = \frac{\sum_{i=0}^{m1}\sum_{j=0}^{m2}\sum_{k=0}^{m3} c_{ijk} X^i Y^j Z^K}{\sum_{i=0}^{n1}\sum_{j=0}^{n2}\sum_{k=0}^{n3} d_{ijk} X^i Y^j Z^K} \end{aligned} \tag{6}$$

where, x, y are the image coordinates, X, Y, Z are the object coordinates, and a_{ijk}, b_{ijk}, c_{ijk}, d_{ijk}, are the polynomial coefficients.

The coefficients of the RFM are called rational polynomial coefficients (RPCs). The RPCs are also referred to as rational function coefficients (RFCs) (Hu and Tao, 2002), or rational polynomial camera coefficients (Grodecki and Dial, 2003). Typically, as the RPCs are selected to the third degree, eighty coefficients are essentially included. There are two approaches to determine the RPCs. The first employs numerous ground control points (GCPs) to derive the coefficients. However, as this approach requires too many GCPs, it is considered unrealistic (Hu and Tao, 2002). The second approach utilizes the satellite on-board orientation, which includes orbital parameters and attitude data in generating enough transformation anchor points. This method achieves a high precision under the circumstances that the on-board orbital parameters and attitude data are accurate. As most high-resolution satellites are equipped with instruments such as GPS, INS, and star trackers, they are capable of providing satisfactory orientation measurements. Accordingly, the second approach is selected in this investigation.

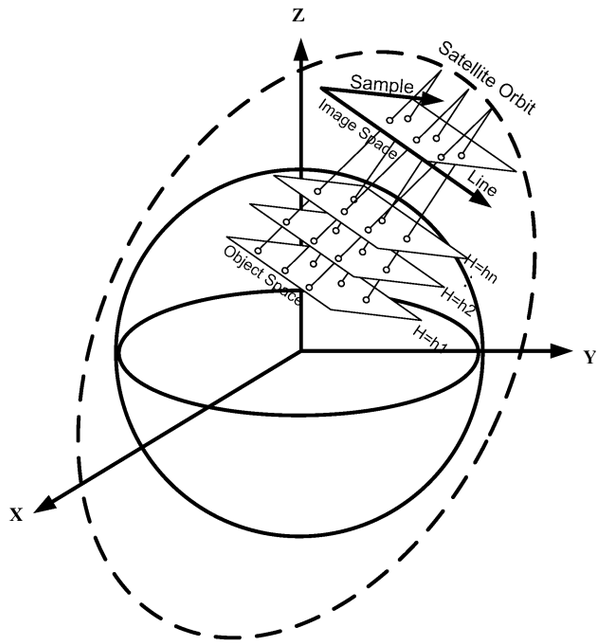

Figure 2. Illustration of VAPs generation.

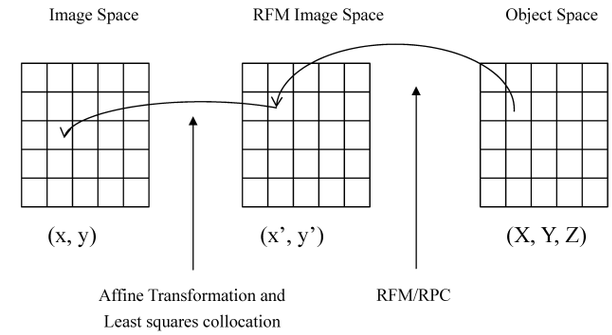

Figure 3. The procedure of mapping sequence for RFM.

The Generation of Virtual Anchor Points

Grodecki and Dial (2003) provided the concept of using satellite on-board data to generate transformation anchor points for the determination of RPCs. In this paper, more technical details will be provided for this procedure. The scheme of the anchor point generation is to determine the image coordinates for a set of multilayer virtual ground points by using satellite orientation parameters. First, we use the satellite on-board data to develop the physical sensor model. Afterwards, we generate numerous three-dimensional grid points in the object space, where they are distributed with different elevations. The corresponding image coordinates for these three-dimensional grid points are calculated by using the physical sensor model. The generated points are called virtual anchor points (VAPs). Figure 2 illustrates the modified representation of Grodecki and Dial (2003) for the geometric concept of VAP generation.

Determination of RPCs

A least squares fitting is applied to determine the RPCs from the large number of VAPs. This is performed by linearizing the RFM with respect to the RPCs, where the observation equations can thus be obtained. Notice that the numerical stability should be assured by using a normalization procedure. A more in depth description of the normalization details, in regards to the RPC determination can be found in Tao *et al.* (2000).

Model Error versus Image Length

Since the RFM is an approximation of the RSM, the analysis for model errors is needed. For a satellite with a specific field of view, the modeling errors may behave differently for along-track and cross-track components. Theoretically, the number of VAPs may also produce different model errors. In addition, as the length of the image strip increases, the model errors should vary as well. Therefore, we will test the errors of the generated RPCs with respect to the number of VAPs and image length, in the next section.

RFM Bias Compensation

In order to compensate the systematic bias of RPCs, we use an affine transformation to correct the error in the image space. The affine transformation coefficients can be calculated from ground control points (Fraser and Hanley, 2003). Afterwards, a 2D least squares collocation in the image space is applied to further correct the local error of RPCs. Figure 3 illustrates the procedure of RFM bias compensation. Starting from the object space, the 3D object coordinates (X,Y,Z) are mapped to the RFM coordinates (x',y') by using the RPCs. The accuracy of the 2D image coordinates (x,y) can thus be adjusted by an affine transformation. A least squares collocation is also considered to minimize the local systematic errors. The approach may be extended to 3D Positioning using stereopairs with some modifications, which include the space intersection in an iteration manner.

Experimental Results

Two FORMOSAT-2 panchromatic strips with different number of scenes are tested in the experiment. The image size of a standard scene is 24 km by 24 km when viewed at nadir. The ground sampling distance for the test images increase from 2.0 m to 2.2 m per pixel, as it has a 17 degree tilt angle. The image strip length is roughly 26 km by 360 km and 26 km by 288 km for Case I and Case II, respectively. It covers an area starting from the northern areas of Taiwan to the southern parts. The location of the test image strips is shown in Figure 4. The object coordinates of GCPs and Independent Check Points (ICPs) were acquired from 1:5000 scale base maps. The accuracy of the coordinates is estimated at 3 meters. The DTM was acquired from the topographic database of Taiwan, and the resolution of the DTM is 40 meters. For Case I, there are a total of 105 test points, 33 of them are used as control points, while the remaining ones are used for validation. For Case II, there are a total of 79 test points, 25 of them are used as control points, while the remaining ones are used for validation. The related information is shown in Table 1.

The experiments include three different aspects in the validation procedure. The first evaluates the accuracy of the RSM. The second checks the accuracy of the RPC, which in turn analyzes the model errors of the RFM/RPC. The third assesses the correctness of the RFM.

RSM Validation

Once the satellite orientation is modeled, we calculate the point of intersection of an image pixel's line-of-sight with the DTM. The accuracy of the RSM may, therefore, be revealed by evaluating the ICPs. Table 2 summarizes the validity for the RSM. Three items are assessed in the orbit modeling. The first

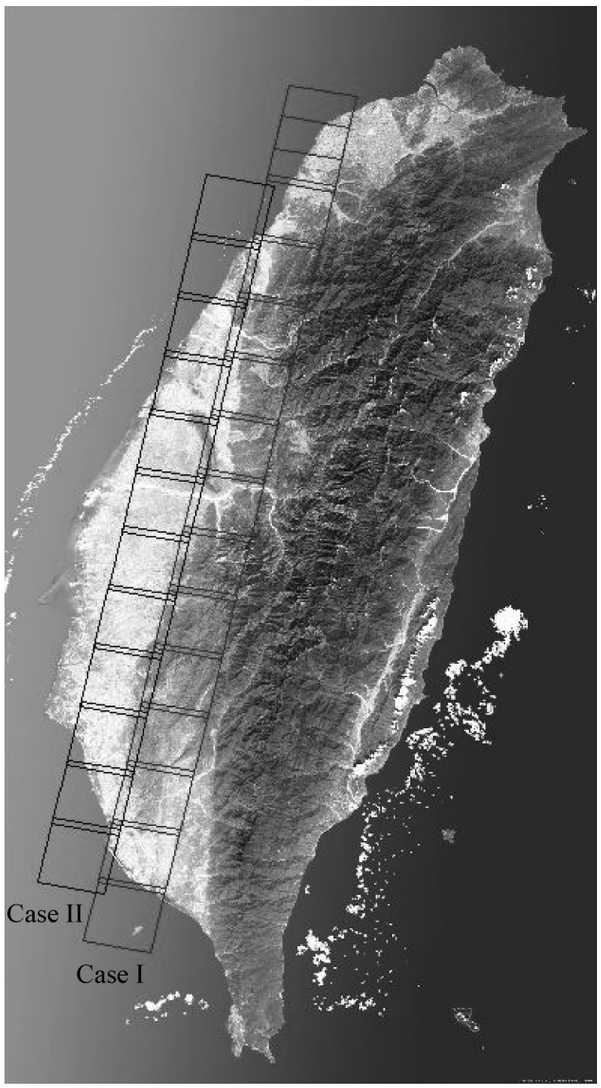

Figure 4. The location of test images. (© CSRCR/CNES, 2002)

TABLE 1. RELATED INFORMATION OF THE TEST IMAGE

Test Data	Case I	Case II
Date	11/11/2004	12/17/2004
No. Scenes per Strip	15	12
Pointing Angle	17°	17°
GSD (meter)	2.2	2.2
Test Area (km*km)	26 * 360	26 * 288
Image size (pixel*pixel)	12000 * 180000	12000 * 144000
No. GCPs/ICPs	33/72	25/54
GCP & ICP Data source	1.5000 topographic maps	1.5000 topographic maps

analyzes the accuracy of the on-board emphasis data, where it does not include any ground control information. The Root Mean Square Errors (RMSE) of Case I in the E and N directions is 44 m and 141 m, respectively. While for Case II, the errors are 33 m and 54 m, respectively; thus, revealing the quality of the on-board data. Notice that there are 15 and 12 scenes in Case I and Case II, respectively. Thus, the average GCP density per standard scene for Case I and Case II are 2.2 and 2.1, respectively. The second studies the correctness of orbit fitting when GCPs and ICPs are employed. For Case I, the RMSE of the ICPs in the E and N directions are 9 m and 14 m, respectively. For Case II, the RMSE of the ICPs in the E and N directions are 16 m and 14 m, respectively. The last item is to evaluate the accuracy after the least squares collocation. For Case I and Case II, the RMSE of the ICPs in the E and N components are reduced to 4.6 m and 4.8 m, respectively. The image resolution is 2.2 m. Thus, the errors are equivalent to 2 pixels in the image scale. The error vector of Case I and Case II after the least squares collocation are shown in Figure 5 and Figure 6. Triangles represent the GCPs, while the circles represent the ICPs.

TABLE 2. ROOT MEAN SQUARE ERRORS OF RSM

Unit: Meters

		GCP		ICP	
Case I	No. GCP/ICP	RMSE E	RMSE N	RMSE E	RMSE N
Before Correction	0/105	0	0	44.11	141.24
Orbit Fitting	33/72	11.84	15.00	9.40	13.68
Least Squares Collocation	33/72	3.12	3.55	4.60	4.79
Case II		RMSE E	RMSE N	RMSE E	RMSE N
Before Correction	0/79	0	0	33.22	54.59
Orbit Fitting	25/54	18.63	15.78	16.63	14.16
Least Squares Collocation	25/54	3.56	4.88	4.66	4.73

RFM Validation

The RFM validation will be presented in two parts. The first examines the model errors for the generated RPCs. In which, we select the Case I, which has a longer strip, in the model error analysis. The second demonstrates the geometrical performance for the RFM using ground control points. Both cases are investigated in the second part.

Model Error Analysis

In order to evaluate the RPC model error, we generate a large number of VAPs to produce the RPCs. The VAPs is split into two groups, where they control and check the RPC generations. Different VAP numbers that are used for checking are applied in finding the suitable number of controlling VAPs, in which, a standard scene is used in this stage. Figure 7 demonstrates the RPC model error when different numbers of the controlling VAPs are utilized. The number of controlling VAPs is between 200 to 50,000. The model error tends to be stable when 5,000 controlling VAPs are employed. The RPC model errors for a standard scene in the sample and line directions are 0.008 pixels and 0.011 pixels, respectively. The sample component is slightly better than the line component.

In addition, as the length of the image strip increases, the model errors should also vary. With this in account, the orbit length is examined and analyzed. The number of scenes differs from 1 to 15. Figure 8 shows that the RPC model error is directly proportional to the orbit length. Nevertheless, the RMSE of the model error for the longest strip is still smaller than 0.15 pixels, as shown in Table 3, proving that their influence is limited.

Accuracy Analysis for Ground Positioning

We use 15 and 12 standard scenes to generate the RPCs for Case I and Case II, respectively. The GCPs and ICPs used in the

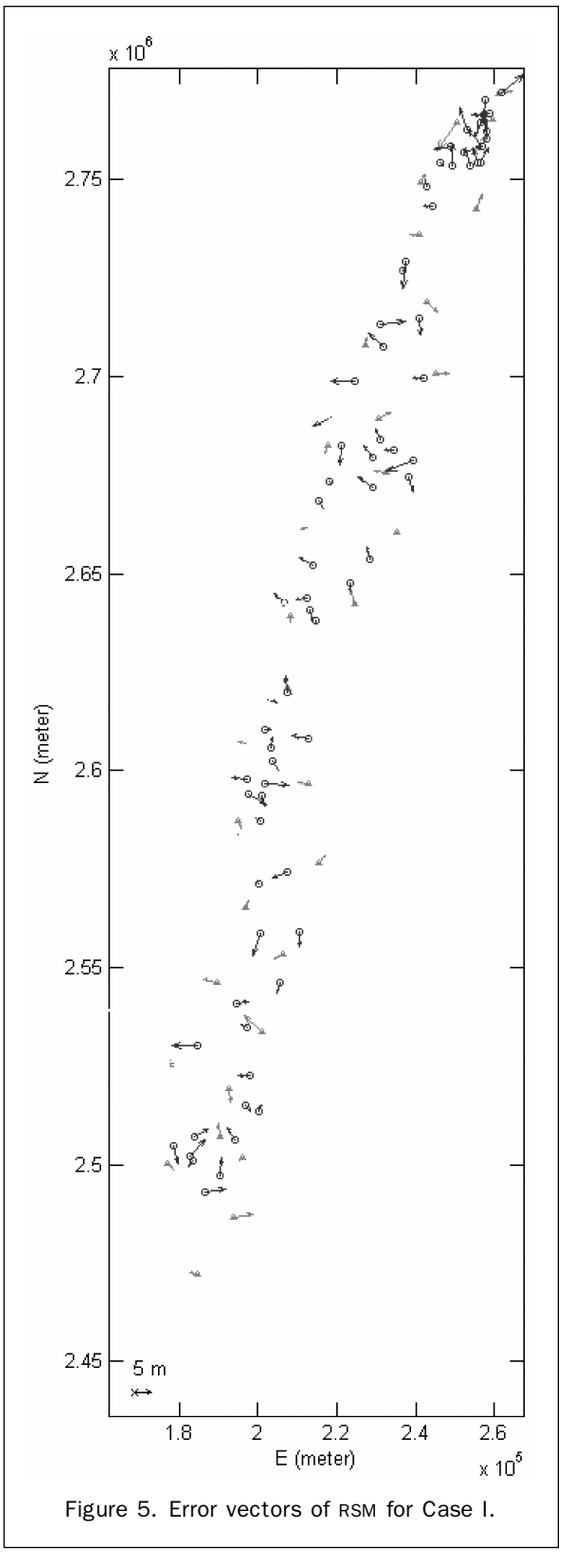

Figure 5. Error vectors of RSM for Case I.

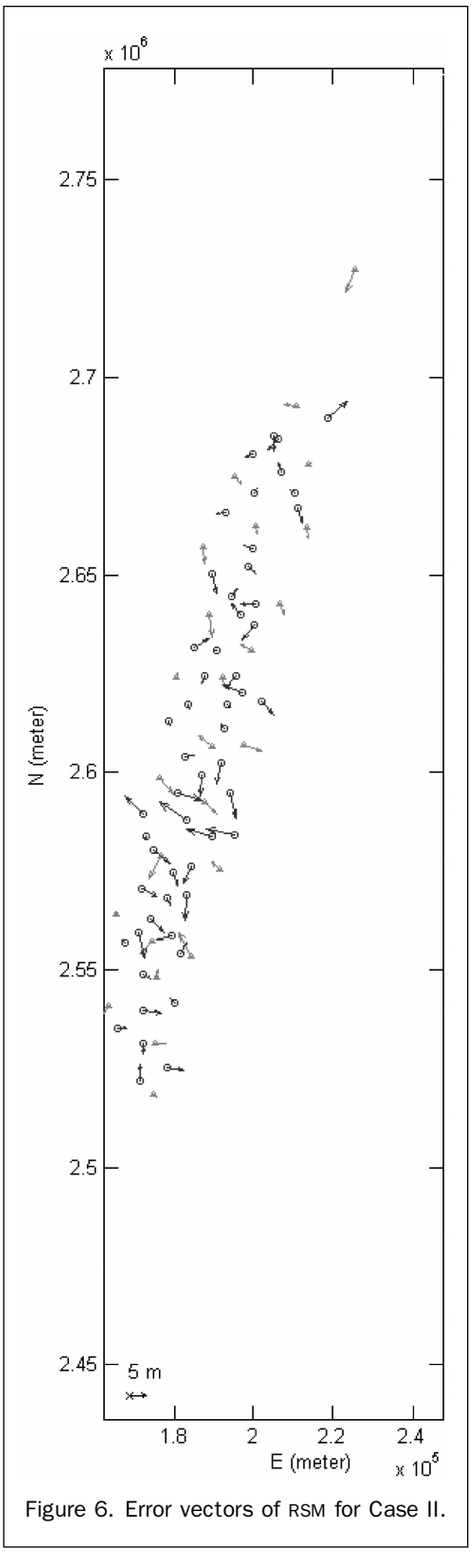

Figure 6. Error vectors of RSM for Case II.

RSM validation are also employed again for the RFM evaluation. First, without the usage of GCPs, the performances of RPCs are tested. This corresponds to the first test in the RSM. The RMSE of RPCs of Case I in the sample and line direction is 21 pixels and 72 pixels, respectively. The RMSE of RPCs of Case II is 16 pixels and 28 pixels, respectively. The assesement is performed in the image space, thus we use "pixel" instead of "meter." Second, for Case I, we use 33 GCPs to perform affine transformation. The RMSE of 72 ICPs is 10 pixels and 19 pixels for the two components, respectively. For Case II, we use 25 GCPs to perform affine transformation. The RMSE of 54 ICPs is 14 pixels and 12 pixels for the two

TABLE 3. RMSE STATISTICS FOR MODEL ERROR OF RPCS

Unit: Pixels

Number of Scene	VAPs per Scene	Check VAPs per Scene	RMSE Sample	RMSE Line	Max Error Sample	Max Error Line
1	3495	3482	0.008	0.011	0.03	0.04
2	7391	7387	0.021	0.034	0.10	0.11
3	10376	10373	0.031	0.052	0.19	0.28
4	12643	12641	0.053	0.058	0.24	0.48
5	14430	14428	0.058	0.060	0.32	0.48
6	15885	15883	0.060	0.064	0.37	0.49
7	17091	17089	0.060	0.070	0.37	0.49
8	18083	18082	0.063	0.088	0.37	0.49
9	18939	18938	0.068	0.097	0.43	0.49
10	19674	19672	0.069	0.113	0.44	0.49
11	20310	20309	0.088	0.114	0.44	0.49
12	20874	20873	0.096	0.121	0.46	0.50
13	21384	21384	0.096	0.127	0.46	0.50
14	21813	21812	0.103	0.128	0.50	0.57
15	22310	22310	0.110	0.138	0.52	0.59

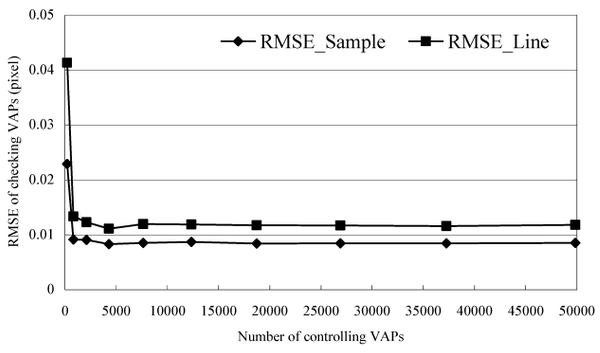

Figure 7. Model Errors of RPCs.

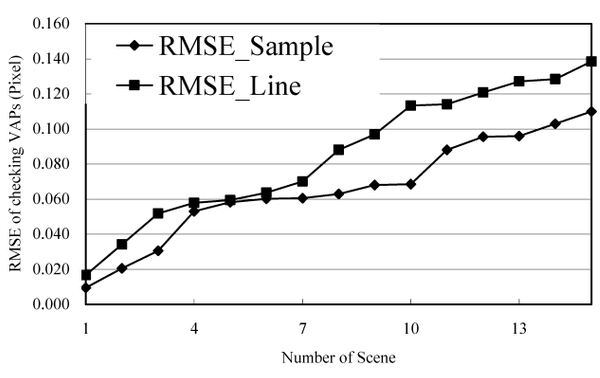

Figure 8. Model Errors of RPCs with different orbit lengths.

components, respectively. This corresponds to the orbit fitting in the RSM as shown in Table 2. Third, we apply the least squares collocation to refine the model. The RMSE of ICPs is reduced to 2.5 pixels for both cases. Figure 9 and Figure 10 are the error vector of RFM after the least squares collocation. Table 4 summarizes the geometrical performance of the RFM.

If we change the dimension from pixel to meter, it is found that the RSM errors in Table 4 are similar to the RFM errors shown in Table 2. This is consistent to the satellite's onboard datasets, before correction, orbit fitting, and least square collocation. The similarity of the positioning accuracy for both methods reveals an insignificant model error of the RPCs.

Summary of the Experimental Results

The experimental results are summarized as follows.

1. The on-board orientation parameters of FORMOSAT-2 could yield 30 to 150 m positioning error on the ground. The error could be reduced to 10 to 17 m when sparse GCPs were employed. Significant improvements are observed when least squares collocation is included. That reveals the local systematic errors are better compensated.
2. The positioning accuracy for FORMOSAT-2 images is around two pixels in this investigation. Notice that the accuracy of the GCPs is estimated at 3 m. Thus, if the quality of the GCPs improves, the higher positioning accuracy is expected.
3. The model errors of RFM/RPC vary with the number of VAPs. Some five thousand points are suggested when the VAPs are uniformly distributed.
4. The model errors of RFM/RPC vary with the length of the strip. The error is 0.011 pixels when a standard scene is tested. The errors may be controlled within 0.15 pixels even when a strip with 15 standard scenes is tested.
5. The RSM behaves slightly better than RFM/RPC in the accuracy check. This is consistent with the small model error of RFM/RPC.

Conclusions

This paper compares the geometric performance between the RSM and RFM for FORMOSAT-2 images. In this investigation, we provide a least squares collocation procedure for the RSM and RFM. The model error of the RFM is also analyzed. Experimental results indicate that the RSM performs just slightly better than the RFM in this study. For a standard scene, the model error between the physical sensor model and the rational function model is 0.01 pixels. For a strip with 15 scenes, the model error increases to 0.15 pixels.

Acknowledgments

This investigation was partially supported by the Remote Sensing Group of the Council of Agriculture under Project No. 93AS-2.5.1-ST-a2. The authors would like to thank the Center for Space and Remote Sensing Research at the

TABLE 4. ROOT MEAN SQUARE ERRORS OF RFM

Unit: Pixels

		GCP		ICP	
Case I	No. GCP/ICP	RMSE Sample	RMSE Line	RMSE Sample	RMSE Line
Before Correction	0/105	0	0	21.22	72.19
Affine Transformation	33/72	12.30	18.45	10.73	19.42
Least Squares Collocation	33/72	0.50	1.60	2.36	2.59
Case II		RMSE Sample	RMSE Line	RMSE Sample	RMSE Line
Before Correction	0/97	0	0	16.03	28.54
Affine Transformation	25/54	15.07	10.03	14.33	12.62
Least Squares Collocation	25/54	0.73	0.63	2.29	2.38

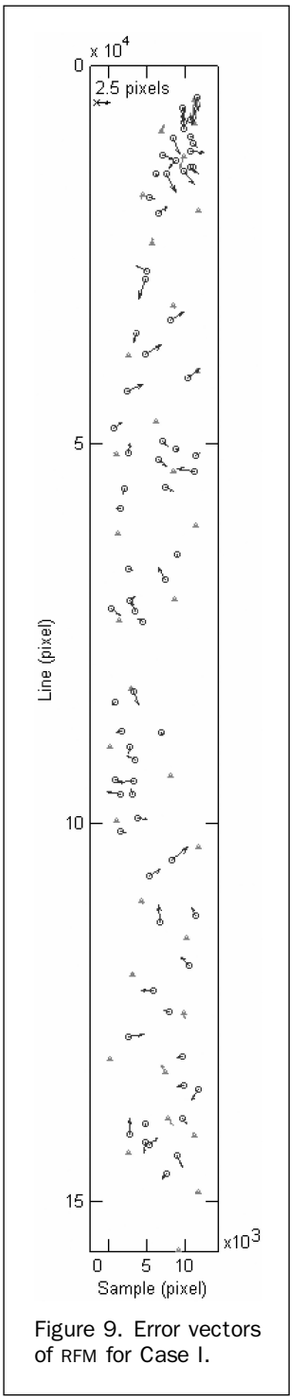

Figure 9. Error vectors of RFM for Case I.

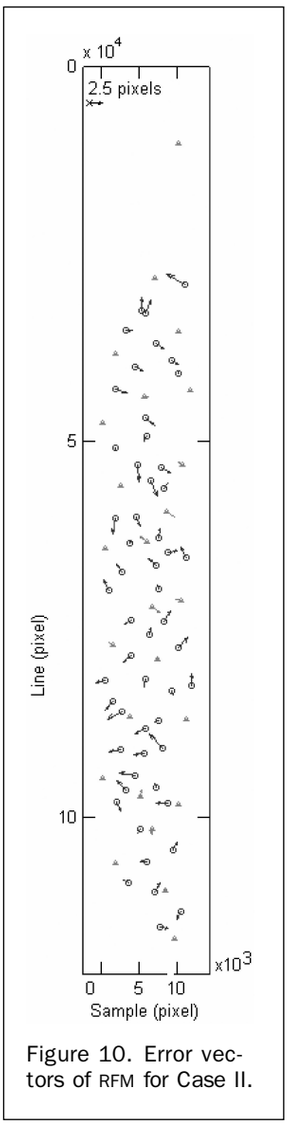

Figure 10. Error vectors of RFM for Case II.

National Central University and the National Space Organization of Taiwan for providing the test data sets.

References

Chen, L.C., and L.H. Lee, 1993. Rigorous generation of digital orthophotos from SPOT images, *Photogrammetric Engineering & Remote Sensing*, 59(3):655–661.

Chen, L.C., and L.Y. Chang, 1998. Three dimensional positioning using SPOT stereo strips with sparse control, *Journal of Surveying Engineering*, ASCE, 124(2):63–72.

Di, K., R. Ma, and R. Li, 2003. Geometric processing of IKONOS stereo imagery for coastal mapping applications, *Photogrammetric Engineering & Remote Sensing*, 69(8):873–879.

Dowman, I.J., and P. Michalis, 2003. Generic rigorous model for along track stereo satellite sensors, *Proceedings of the ISPRS Workshop on High Resolution Mapping from Space*, 06–08 October, Hanover, unpaginated CD-ROM.

Fraser, C.S., and H.B. Hanley, 2003. Bias compensation in rational function for IKONOS satellite imagery, *Photogrammetric Engineering & Remote Sensing*, 69(1):53–57.

Grodecki, J., and G. Dial, 2003. Block adjustment of high-resolution satellite images described by rational polynomials, *Photogrammetric Engineering & Remote Sensing*, 69(1):59–68.

Hu, Y., and C.V. Tao, 2002. Updating solutions of the rational function model using additional control information, *Photogrammetric Engineering & Remote Sensing*, 68(7):715–723.

Li, R., 1998. Potential of high-resolution satellite imagery for national mapping products, *Photogrammetric Engineering & Remote Sensing*, 64(2):1165–1169.

Mikhail, E.M., and F. Ackermann, 1982. *Observation and Least Squares*, University Press of America, New York, 401 p.

NIMA, 2000. *The Compendium of Controlled Extensions (CE) for the National Imagery Transmission Format (NITF)*, STDI- 0002, Version 2.1, 16 November.

NSPO, 2005. FORMOSAT-2 Remote Sensing Mission, URL: http://www.nspo.org.tw/e60/menu0403.html, (last date accessed: 13 February 2006).

Robertson, B.C., 2003. Rigorous geometric modeling and correction of Quickbird imagery, *Proceedings of the International Geoscience and Remote Sensing Symposium*, 21–25 July, Toulouse, France, unpaginated CD-ROM.

Tao, C.V., Y. Hu, J.B. Mercer, S. Shenick, and Y. Zhang, 2000. Image rectification using a generic sensor model – rational function model, *International Archives of Photogrammetry and Remote Sensing*, XXXIII(B3), Amsterdam, pp. 874–881.

Tao, C.V., and Y. Hu, 2001. A comprehensive study of the rational function model for photogrammetric processing, *Photogrammetric Engineering & Remote Sensing*, 67(1):1347–1357.

Toutin, T., 2003. Error tracking in IKONOS geometric processing using a 3D parametric model, *Photogrammetric Engineering & Remote Sensing*, 69(1):43–51.

Toutin, T., 2004. Geometric processing of remote sensing images: Models algorithms and methods, *International Journal of Remote Sensing*, 25(10):1893–1924.

Westin, T., 1990. Precision rectification of SPOT imagery, *Photogrammetric Engineering & Remote Sensing*, 56(2):247–253.